AN ABSTRACT OF THE THESIS OF

Vanessa L Adriatico for the degree of Master of Science in Radiation Health Physics presented on May 26, 2022.

Title: Characterization of Radionuclide Resuspension via Aeolian Processes at the Ambrosia Lake West Mill Facility

Abstract approved: _____

Camille J. Palmer

The Ambrosia Lake West Site is a former uranium recovery facility located north of Grants, New Mexico. It currently serves as a uranium mill tailings site undergoing reclamation and decommissioning. High velocity winds are common in the area, causing soil erosion via aeolian processes. Strong winds may carry soil for several kilometers which is redeposited downwind. This study estimates the potential for impact on remediation efforts caused by downwind contamination from soil-bound radionuclide resuspension. The study was performed by measuring the mass of soil moving onsite to determine horizontal saltating flux over the period of 3 months. Previous frameworks relating dimensional flux were used to estimate suspension flux from site-massed saltating flux. Utilizing concentrations of soil-bound radionuclides and meteorological data collected onsite, a modified Gaussian plume model estimating downwind deposition of contaminants was constructed.

The highest deposition rate reported suggests millions of years of deposition are required to exceed the criterion for release, far longer than the anticipated release of the site in 2030. Based on the results, estimated impacts of wind-blown soil contamination were determined to be negligible.

Characterization of Radionuclide Resuspension via Aeolian Processes at the Ambrosia Lake West Mill Facility

by

Vanessa L Adriatico

A THESIS

submitted to

Oregon State University

in partial fulfillment of
the requirements for the
degree of

Master of Science

Presented May 26, 2022
Commencement June 2022

Master of Science thesis of Vanessa L Adriatico presented on May 26, 2022.

APPROVED:

Major Professor, representing Radiation Health Physics

Head of the School of Nuclear Science and Engineering

Dean of the Graduate School

I understand that my thesis will become part of the permanent collection of Oregon State University libraries. My signature below authorizes release of my thesis to any reader upon request.

Vanessa L Adriatico, Author

ACKNOWLEDGEMENTS

I would like to thank my advisor, Dr. Camille Palmer, for guiding me throughout my graduate school experience. I will carry her personal and professional advice with me through the rest of my career. I would also like to acknowledge my exceptional graduate committee who have supported me both in and outside the classroom. I'd like to thank Dr. Natasha Mallette for being an exceptional role model and mentor.

I would also like to extend my deepest gratitude to the entire staff of H3 Environmental, especially Mike Schierman, without whom I wouldn't have had a master's thesis. I will always remember my summer in New Mexico fondly. I extend this sentiment with great sincerity to BHP, especially Dr. Liz Ruedig, for supporting my research and allowing me access to the site. I was able to present at my first conference with your support.

Finally, I'd like to thank my friends and family. Through the support of my parents and sisters, I know am able to accomplish whatever I set my mind to. To Abby, Sophie, and Mitch, I would have not nearly enjoyed my time in Corvallis as much as I have without your friendship. Thank you to my brilliant best friends, Allie and Mikey. My most special thanks are to Avery, who was with me every step of the way through my academic journey. I'm so excited for what's to come.

TABLE OF CONTENTS

TABLE OF CONTENTS (Continued)

LIST OF FIGURES

LIST OF TABLES

LIST OF APPENDIX FIGURES

LIST OF APPENDIX TABLES

Nomenclature

BSNE Big Spring Number Eight

DOE United States Department of Energy

EPA United States Environmental Protection Agency

HMF Horizontal Mass Flux

IMF Integrated Mass Flux

LTSM Long-Term Surveillance and Maintenance

NORM Naturally Occurring Radioactive Material

NRC United States Nuclear Regulatory Commission

RAML Rio Algom Mining LLC

TENORM Technologically Enhanced Naturally Occurring Radioactive Material

TPU Total Propagated Uncertainty

VMF Vertical Mass Flux

Chapter 1: Introduction

Radioecology is a broad and multidisciplinary field that intersects radiation physics and environmental science. It investigates the movement of radionuclides through the environment and how it may affect biota. One significant means of radionuclide transport is via wind-driven resuspension in which air motions can pick up and carry radionuclides to other locations.

The Ambrosia Lake West disposal site located northwest of Grants, New Mexico (See Figure 1.1) is one such site where atmospheric transport of radionuclides is of concern. The Grants Uranium District was at one point the most active in the United States, beginning in the early 1950s up until the uranium market collapse in the early eighties [26]. The former uranium mill and recovery facility was built by the Kerr-McGee Nuclear Corporation and its partner, Phillips Petroleum Company in 1957. Uranium ore obtained from nearby mines was processed from 1958 to 1963 in the mill, when the facility was purchased by United Nuclear Corporation. By the late 1970s, the United Nuclear Corporation rededicated the facility towards recovery of uranium through mine water via ion-exchange. All operations at the facility ceased in 1982.

While the mill facility has been inactive since, the site is still undergoing decommissioning and cleanup. There is a large impoundment at the Ambrosia Lake disposal site that contains 33 million tons of radioactive mill tailings that cover ap-

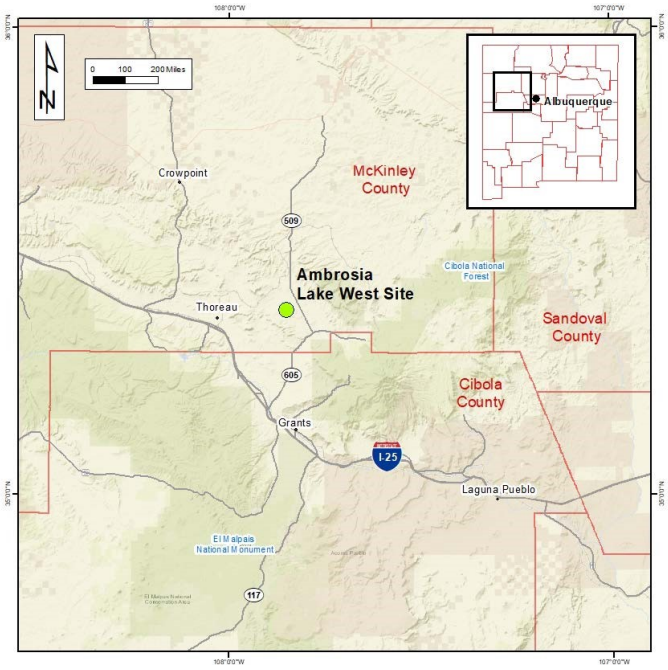

Figure 1.1: Map of the Ambrosia Lake Area
[8]

proximately 370 acres of land. Tailings are a sandy processed waste material from the uranium mill that consists of uranium ore residues. Windblown tailings from the impoundment transport radionuclides onto nearby soil. The radionuclides of concern onsite are uranium-238, thorium-230, radium-226, and radon-222. These are all naturally occurring radioactive materials (NORM), but interference from mining has created technologically-enhanced naturally occurring radioactive materials (TENORM) which are more concentrated or accessible to environmental exposure.

The United States' Nuclear Regulatory Commission (NRC) lists the extent of

windblown soil contamination on and potentially off-site as a major issue at the facility [8]. The facility was purchased in 2001 by Rio Algom Mining, LLC with the intent to decommission and reclaim the site. The site was declared inactive in 2002 and the mill was demolished in 2003 [1]. Tailings from when the facility was operational have been disposed of either within the tailings impoundment or onsite in one of two disposal cells (See Figure 1.2).

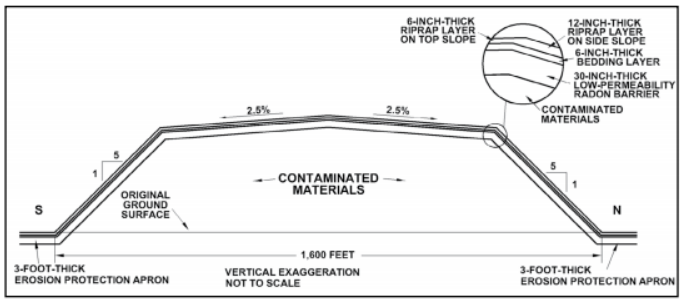

Figure 1.2: North-South Cross Section of a Disposal Cell at Ambrosia Lake [8]

Soil affected by windblown tailings is expected to be placed in a cell that has yet to be submitted to the NRC. There is the additional potential for remediated parcels of land to be recontaminated by proximal unremediated sections or from the tailings pile itself.

Climate patterns will affect the atmospheric transport of radionuclides at the Ambrosia Lake facility. The site is sparsely vegetated with a semi-arid climate and receives approximately six to nine inches of rainfall annually based on available site-specific meteorological data. The soil type onsite is fine loamy sand [30]. The average wind speed is approximately 3.35 meters per second prevailing in the SSW

direction. The average temperature between the two 2 and 10 meter sensors was approximately 16.97 degrees Celsius (62 degrees Fahrenheit) and average relative humidity was approximately 37.39%.

Given the circumstances of the study and the climate at Ambrosia Lake, it is appropriate to employ the principles of Aeolian processes relating to wind erosion to characterize sediment transport. Aeolian studies relate the motion of wind to transport and deposition of sediments. It is three-dimensional, with horizontal mass flux characterizing sediment saltation and vertical mass flux characterizing sediment suspension. A commonly used sampler used to study Aeolian transport is the Big Spring Number Eight (BSNE) sampler designed by DW Fryrear [12]. The BSNE sampler is a rugged, passive sampler that orients itself upwind to collect blown sediment used to determine horizontal mass flux. Vertical mass flux of wind-blown sediments can be directly measured, but requires substantial resources and infrastructure to do so [38]. At remote sites such as the mill facility where electricity is unavailable, it is more effective to estimate vertical flux based on its relationship to horizontal mass flux.

Horizontal mass flux was sampled at two locations from July 16th, 2021 to September 27th, 2021. A background sample site was chosen to be consistent with the United States Environmental Protection Agency (EPA) background monitoring locations which serves as comparison to an unremediated section sampling site. The unremediated sampling site was chosen for its ease of access and environmental conditions that are ideal for dust sampling, namely soil quality and presence of vegetation. A meteorological station nearby recorded site weather and atmospheric

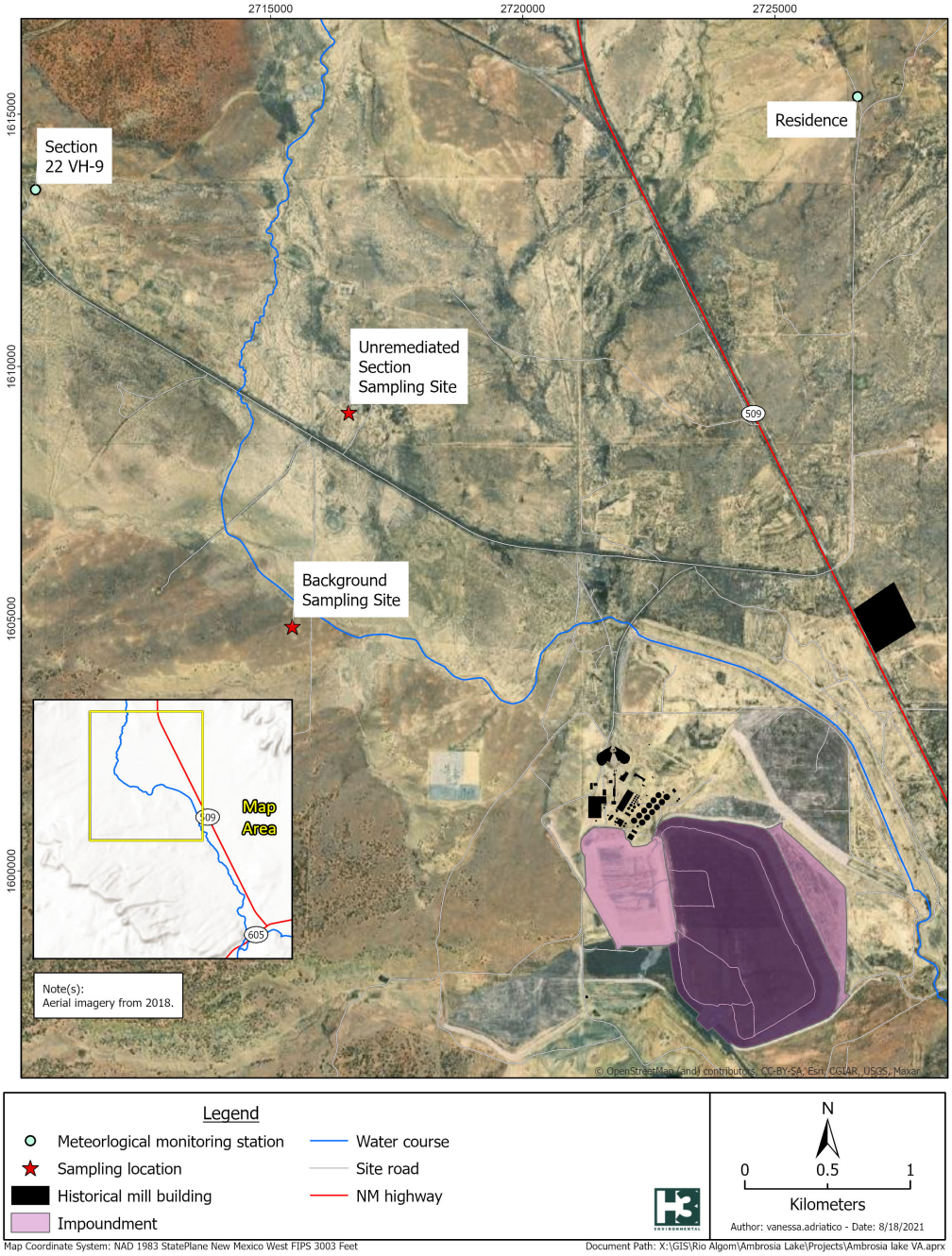

Figure 1.3: Map of Ambrosia Lake Site and Sampling Locations

conditions, recording once hourly over the span of the sampling period (See Figure 1.3). Downwind deposition models were then created and analyzed for potential impacts onsite.

1.1 Research Objective

The purpose of this study is to utilize previous frameworks relating aeolian processes to resuspension of radionuclides to determine the impacts of down-wind radionuclide deposition onsite. This is a particularly important consideration at locations such as the Ambrosia Lake West mill facility where active remediation efforts take place. Recontamination via wind-blown radionuclides would stall decommissioning and incur additional cleanup costs. Workers may also find themselves in areas believed to be remediated but are not. To promote an efficient safety-culture, it is critical to understand all potential pathways of radionuclides and what risks are posed.

Sampling for the study occurred during a period of low-remediation. Choosing a time frame with low human interference reduces the amount of activity in which dust is suspended, allowing for a more accurate measurement of ambient soil transport. Soil samples to quantify deposition via aeolian processes were collected and used to estimate resuspension rates. Using historic soil concentration data and meteorological data, a model was constructed to determine impacts of wind-blown radionuclides under ambient conditions at the Ambrosia Lake West mill facility.

Chapter 2: Literature Review

2.1 Introduction to Aeolian Processes

Aeolian processes are named after Aeolus, Greek guardian of the winds. Aeolian studies examine how wind-flow contributes to soil and sediment transport - and how land formations and erosion occur as a result. Aeolian transport depends on the size (diameter) of the sediment and velocity of the wind.

Ralph Bagnold was the first to provide a comprehensive study of sand transport in his 1941 book, "The physics of wind-blown sand and desert dunes". Yaping Shao's 2008 "The physics and modeling of wind erosion" provided updates to Bagnold's work and the two books serve as foundational aeolian literature to this day [33]. Bagnold categorized three main forms of aeolian transport, surface creep, suspension, and saltation [3].

Saltation is derived from Latin verb *salire*, which means "to leap". The BSNE sampler is designed to capture saltating particles [27]. Naturally, saltation characterizes sediment transport for soils which wind will momentarily lift sand into the air until it comes crashing back down (in a "leaping" motion). Saltation occurs for sediments with a diameters of approximately 70 - 500 μm and upon impact serves to mobilize both larger and smaller sediments (which will transport via creep, suspension, or elicits further saltatory action) [20]. Horizontal flux is also sometimes

referred to as saltating flux [39].

For sediments approximately 70 μm in diameter and smaller, the primary mode of transport is suspension. Transport via suspension is characterized by uplift of sediments that are carried into the air for extended periods of time. Suspended soil may travel very far distances, up to thousands of kilometers from the source term [20]. For the purposes of this project, understanding transport of radionuclides attached to suspended soils is critical to the characterization of potential recontamination. This places importance on vertical, or suspended, mass flux [39].

Surface creep is a phenomena in which larger sediment particles are too large (diameters of approximately 500 μm or greater) and heavy to saltate or suspend, so they roll or *reptate* short distances across the the soil surface until arrested by either larger particles or other obstructions such as vegetation or land formations [20].

As this study intersects aeolian and radioecologic studies, it warrants a brief definition of terminology. In wind erosion studies, *suspension* refers to the indefinite lift of particles or sediments into the air. In radioecology, *resuspension* refers to settled radionuclides on the ground being lifted into the atmosphere. The two terms are related, although not identical in definition.

2.1.1 Factors Influencing Site Erosivity

The presence of vegetation will heavily influence site erosivity, with horizontal mass flux demonstrating a strong dependency on vegetation cover distribution. Average

horizontal mass flux decreases as grass cover increases [22]. Wind-flow patterns affecting soil erosion can also change depending on the height, width, and porosity of vegetation. An increase in any of the aforementioned factors will weaken the relationship between the two [39]. Soil stability largely factors into site erosivity - a well maintained soil retains nutrients and does not degrade rapidly. Breshears et al. observed a greater inherent likelihood in wind-blown sediment transport for undisturbed shrubland sites than other ecosystems based on vegetation cover affecting wind-flow [6]. The dryness of soil, relatively undisturbed environment, and light vegetation cover in the site's desert grassland lend to conditions ideal for wind erosion and subsequent radionuclide resuspension to occur.

Environmental disturbances may remove vegetative cover and increase erosion by orders of several magnitudes [38].These disturbances may occur naturally, such as earthquakes, storms, fires, or other disasters, or by cause of human activity such as mining. The study takes place in sites where no active remediation is taking place and very little interference occurs that would increase suspension or disturb vegetation. This allows for a more accurate estimation of ambient resuspension and deposition rates onsite.

2.1.2 Threshold Wind Velocity

Fluid and impact thresholds determine the minimum wind velocity in which saltation will initiate and cease, respectively. Models of soil transport are dependent on these threshold velocities to predict downwind deposition. Threshold shear

wind stress (minimum wind speed required for wind-driven soil transport) further determines the frequency of soil erosion and dust emission, particularly in desert and semiarid environments [25]. Published models determining sand transported by wind based on a predicted threshold velocity have varied widely from observed transport rates. Dong et al. reports the ratio of predicted to field transport rates may range anywhere from 0.65 to 300 [9]. Predicted soil transport rates (and mass fluxes) are often based on wind-tunnel experiments, where conditions are ideal for soil transport and unrealistic in practice. Though threshold saltation is critical in determining soil flux, there is no central consensus on how to best determine a threshold: both empirically measured or through modelling [4]. Models studying saltation transport would historically use only the fluid threshold for shear stress [18].

Many present-day models use impact threshold alone - using both impact and dynamic thresholds together is far less common. Recent publications have argued for the need for both fluid and impact thresholds as observed wind patterns are often turbulent rather than uniform [25]. Due to limitations of modeling software, this study utilizes a separate threshold, the dynamic shear stress threshold, which is the minimum wind velocity in which saltation is sustained. The dynamic shear stress threshold was set to 1 cm/sec, which comes at recommendation of the U.S. Department of Energy's suggested deposition velocity for emergency radiological responses regarding unfiltered, nontritated releases [36]. pa

2.2 Radionuclides of Concern

The uranium-238 isotope is naturally occurring in the form of ore deposits found in the Earth's crust. It has a high relative abundance (99%) in comparison to other uranium isotopes. Its decay chain is often referred to as the radium series as U-238's fifth progeny is a relatively long lived radium isotope: radium-226. Given the site's history as a natural uranium mine and mill, the radionuclides of concern are part of the radium decay series.

For release of a parcel of land at the facility, compliance with 10 CFR 40, Appendix A, Criterion 6(6) is required. This regulation posits that for a 100 square meter area of land (referred to as a "grid") to be released, in the first 15 centimeters of soil, the concentration of Ra-226 cannot be in excess of background levels by more than 5 picoCuries (pCi) per gram (g). This criterion of concern will be used as an indicator of whether deposition occurring onsite has impact. Should ground deposition onto a grid change Ra-226 concentrations to be in excess of the criterion in a reasonable period of time, then resuspension via aeolian processes are of concern onsite.

2.3 Review of Published Radionuclide Resuspension Studies

There are two contexts in which resuspension of radionuclides have been historically studied: exposures resulting from resuspended fallout following above-ground nuclear weapons testing and nuclear power plant accidents [39]. The foundation of both these studies are rooted in wind erosion via aeolian processes, though re-

suspension studies progress independently from aeolian scholarship. Soil erosion studies were first conducted in an agricultural context, when interest in the subject rose after the occurrence of the Dust Bowl in the United States [39][2]. Aeolian research is pioneered by the likes of Kok, Bagnold, and Fryrear who determined the factors determining soil transport, how to measure soil erosion, and devised models to estimate potential erosive events.

Early (prior to the late 1950s) resuspension studies were poorly documented and serve only as a general basis for information rather than providing more detailed results [2]. One of the critical elements of the fallout resuspension studies of this era is time, given the need to know the intensity of dose exposure and how time post-detonation may affect exposure. Research was motivated largely by the sociopolitical climate following the second World War [2]. The results of these studies return to two of the three principles to reduce exposure to radiation that health physicists abide by: time and distance. In these early studies, as time passes, the concentration of radionuclides in the air will decrease exponentially post-detonation. The further one is from a detonation, the less likely they are to be exposed to air-entrained radionuclides.

Some of the earliest documented approaches towards characterizing resuspension defined a resuspension factor, S_f. Langham in 1971 defined it as the following [21].

$$S_f = \frac{\text{Resuspended air concentration(activity per meter cubed)}}{\text{Surface deposition(activity per meter squared)}} \tag{2.1}$$

This is under the assumption that all resuspended air concentration is directly suspended from the local surface area. Langham's model, however, failed to account for variables which affect resuspension such as environment, meteorological conditions, and soil conditions. Two 1964 publications by Stewart and Mishima, respectively published calculated values for S_f based on experiments with conditions undergoing artificial disturbances derived from measurements from detonation events [35] [28].

In 1975, Anspaugh published early models to characterize transport of soil-bound plutonium via resuspension but argued for a greater need to implement soil concentration impacts from weathering [2]. As time progressed and global politics shifted attention from the Dust Bowl and WWII, resuspension studies have too shifted focus from above-ground testing to response on the effects of the nuclear power plant accidents at Fukushima and Chernobyl: particularly from fallout.

Rosner and Winkler's 2001 work sought to determine long-term deposition rates in southern Germany following the Chernobyl accident. Their research found that deposition to soil from suspended radiocesium increased soil concentrations by a magnitude of 4-5. The plume source, from Chernobyl, was able to carry suspended radionuclides from fallout towards Germany and deposit measurable amounts of cesium [32].

Garger et al. constructed long-term predictive models to determine air concentrations of Cs-137 in the Chernobyl exclusion zone from mobilized contaminated dust carried by winds, human activity, and other emission sources. The model

took care to account for temporal variations, annual variations, and identification of general trends and fluctuations to create a reliable model after sampling for approximately four years [14]. Ultimately, this work suggests that with sufficient sampling time, a model can reliably predict movement of radionuclides via aeolian processes at a given site.

Kajino et al. assessed the long-term effects from radioactivity in the atmosphere following the Fukushima disaster from resuspension of radiocesium via dust emission. Previous studies estimated resuspension based on surface air concentrations, pulling from Garger et al.'s work in long-term assessment following from the Chernobyl accident [17]. Kajino et al. used 3D modeling based off of collected data on dust emissions in the contaminated area alongside air concentration measurements - circling back to Langham's original resuspension factor. Simulations were run in bare-soil environments, forests, and in environments where resuspension could occur from buildings or debris around the Fukushima power plant site. The study ultimately found great variation in resuspension based upon climate and vegetation presence and need for further studies on the effects of weathering [19].

Weathering is a phenomena in which downward migration of radionuclides in soil over time influences the activity concentration of resuspended soil. For long-lived radionuclides, weathering will cause a decrease in activity suspended to air more than physical decay. Nicholson evaluated wet and dry deposition, resuspension, and weathering rates in England following a plume passage originating from the Chernobyl accident, estimating deposition velocities based on field measure-

ments taken from a site where deposition from the Chernobyl plume was known. Nicholson found weathering impacts small enough to be insignificant [31]. It will be assumed onsite that weathering impacts are negligible.

Resuspension factor findings from empirically-derived studies are largely site-specific due to the number of variables that influence resuspension. Indeed, it is very difficult to create a general model of resuspension as a function of time that applies to all terrains; this is particularly true given the large range of resuspension factors that are dependent on location [23]. Ultimately, there is still not enough information presented to link both aeolian and resuspension studies in a way that allows us to make general statements about wind-blown soil deposition.

The Whicker et al. 2021 publication attempts to address the lack of a general model that joins aeolian and resuspension studies together. The majority of publications in the past have been site-specific and pertinent to weapons-testing. Whicker et al. sought to develop a theoretical framework to allow for generalized resuspension methods dependent on environmental conditions and the disturbance causing suspension by linking together lessons learned from both aeolian and resuspension studies. The authors also factor in weathering effects to this model. This thesis draws upon the framework to create resuspension and deposition models based off aeolian processes.

2.4 Relationship between Horizontal Mass Flux and Vertical Mass Flux

Gillette et al's 1972 publication first observed simultaneous vertical and horizontal flux flow during saltation, suggesting a relationship exists between the two. The authors were then able to calculate vertical flux using very fine suspended sediments (aerosols). This work was further refined by Shinn et al. in 1974 by normalizing vertical flux of height z to a height of one meter, finding a consistent power law distribution of aerosol concentration and height at wind velocities high enough to sustain saltation [34].

While observations determined a fundamental relationship existed between horizontal mass flux and vertical mass flux, defining this relationship has not been as clear. There is no consensus on any function that can best relate horizontal and vertical mass flux. Farrell's dissertation argues that bias from wind tunnels, which are set in ideal conditions, will not translate to applications on sites where meteorological parameters and wind velocities are variable. In practical applications, there is no uniformity in terrain conditions. Wind tunnels also lack the ability to account for introduced environmental disturbances that may be observed in practice [11].

2.4.1 Calculating Horizontal Mass Flux and Vertical Mass Flux

To calculate horizontal mass flux (HMF), one uses the following equation:

$$HMF = \frac{m}{A * t} \tag{2.2}$$

Where:

- m = sediment mass
- A = area of sampler opening
- t = sampling duration

The area of a BSNE sampler opening is ten square centimeters.

Determining a site's vertical mass flux is a different affair - it can be measured directly but requires using the vertical-gradient method, which is resource-intensive. Without access to electricity on the remote site locations, it's more practical to estimate vertical mass flux using the framework of Whicker et al. in which vertical mass flux is estimated by multiplying a measured mass flux by an appropriate emission factor [39].

2.5 Review of Published Emission Factors

Whicker et al.'s 2021 framework estimates vertical mass flux as the product of horizontal mass flux multiplied by an emission factor appropriate for the environment and setting of the model. An emission factor is defined as the ratio of vertical to horizontal mass flux [39].

Breshears et al. built a conceptual framework for determining vertical mass flux in dryland areas based on the percentage of woody plant canopy cover. Five

ecosystem categories were defined: desert and grassland, shrubland, woodland, and forest. Desert and grassland are distinct ecosystem types but are partnered together as both had low canopy cover; the two are differentiated by types of vegetation and climatic conditions. Central vertical mass flux values were measured for each ecosystem under undisturbed and disturbed conditions. Breshears et al. found an emission factor ratio of 5% [6].

Field data provided by Whicker et al. and a mathematical perspective presented by Kok et al. in 2012 suggest large variations (several orders-of-magnitude) in emissions factors across locations[20][38]. Both suggest that an emission factor of 1% is likely more appropriate to apply broadly to suspension models [39]. For this study, an emission factor of 5% will be applied to allow for a more conservative estimate of vertical mass flux.

2.6 Modeling with CAP-88

Anspaugh described the ideal model for resuspension studies which based itself in flux measurements of moving soil, contamination levels, and environmental conditions such as soil type, climate, and vegetation [2]. Thirteen years later, the Environmental Protection Agency (EPA) released the Clean Air Act Assessment Package (CAP-88), which accounted for such variables. CAP-88 was released as a modeling tool to maintain regulatory compliance with the National Emission Standards for Hazardous Air Pollutants (NESHAP).

CAP-88 allows for estimating average dispersion of radionuclide sources from a

plume. Six radionuclides can be modeled at one time, assuming they are all from the same source term. Two source term types are available in CAP-88: an elevated stack source of a given height or a uniformly contaminated area. Based upon the sources and plume type, the program is able to model radionuclide concentrations in air and deposition on the ground, vegetation, and dose rates to people from ingestion of contaminated food or inhalation. Dose and risk estimates are only for low-level chronic exposures, not acute releases. All-pathway dose risk assessment can be for a population (either provided by CAP-88 or input into the model) or to a maximally-exposed individual. Concentrations in food are based upon food chain models from the NRC Regulatory Guide 1.109 [24].

CAP-88 requires inputs to account for environmental and climactic conditions, such as annual precipitation, ambient temperature, humidity, and altitude of the troposphere mixing layer. Reference cities' wind-files are provided to represent particular environments, including Grants, New Mexico, where the site is located.

The area of assessment for a CAP-88 model is circular with a radius of 80 kilometers. The circle is divided into 16 wedge-shaped sectors that are grouped by cardinal, intercardinal, and secondary intercardinal directions.

2.7 Radionuclide fate and transport

CAP-88 uses a Gaussian plume-type model system to characterize downward dose and deposition of a source term. The Gaussian plume model describes an atmospheric release of radionuclides from a source term, with deposited pollutants

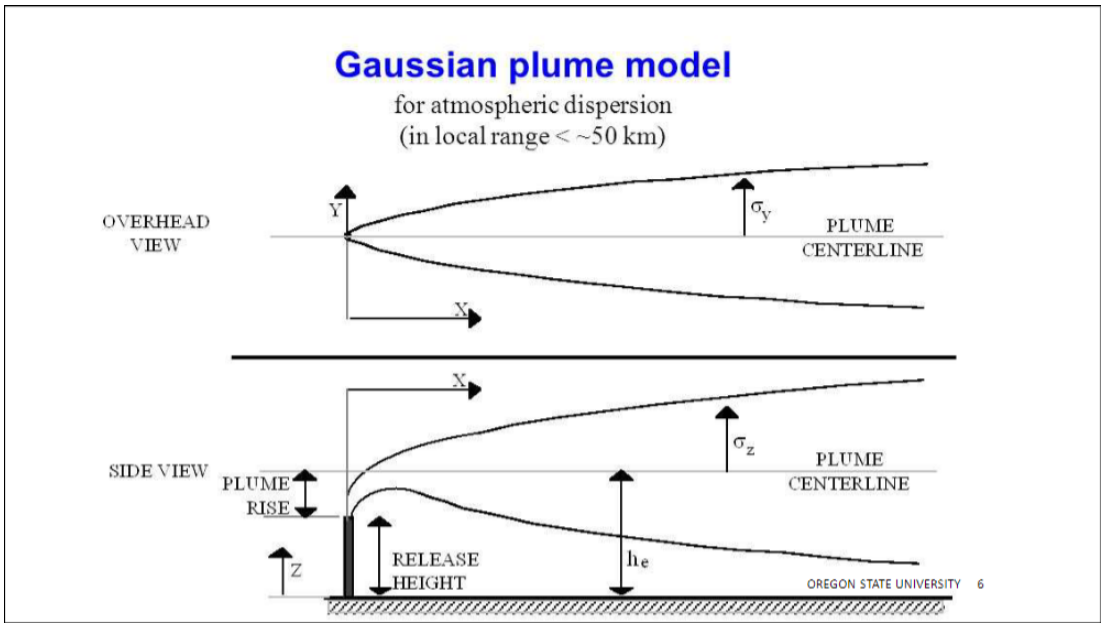

Figure 2.1: Visualization of a Gaussian Plume Model
[16]

taking on a Gaussian distribution both laterally and vertically at any given downwind distance along the plume from its original release. Typical design for a plume model includes a stack source term of a given height in which an initial vertical wind velocity will uplift and form a plume subsequently carried both vertically and horizontally in the wind-stream. The plume rise mechanism must be set to either momentum (quantified by exit velocity in meters per sec) or buoyancy-driven (quantified by heat release rate in calories per sec).

In reality, plumes are rarely perfectly Gaussian when looked at instantaneously (See Figure 2.1); they are impacted by wind fluctuations however, we are more interested in the time-averaged concentration downwind of the release to determine

potential deposition impacts. Temperature inversions may complicate the plume by reflecting it onto itself as air mixes due to differences in air pressure and density. Plumes may also reflect back onto itself when colliding with a physical boundary such as solid ground, buildings or vegetation. These structures may also alter the jet-stream by creating drafts that allows accumulation of contaminants through changes in air pressure. Some radionuclides may deposit and attach to soil or plants while the rest of the plume reflects back onto itself. It is important for a model to account for complications that may affect the plume in order for it to be a proper representation. [16]

Chapter 3: Materials and Methods

3.1 Sample Collection

BSNE sampler installation took part on July 16th, 2021. Two locations were determined: the Unremediated Section Sampling Site (UR) and the Background Sampling Site (B). The UR site was chosen to be representative of a contaminated area. It is located in a sparsely vegetated area with an arid climate which is susceptible to wind erosion. The B site was chosen to represented an uncontaminated area and serve as a nearby control. The EPA uses proximal locations to the B site to perform background measurements as well. The B site is lightly vegetated with grasses and is occasionally grazed by cattle. A small barbed-wire fence was erected around the B site samplers to prevent interference by animals, though no tracks or traces of animals were observed during the course of sampling. The wire fence allowed sediment flow to reach the BSNE sampler and is assumed to have negligible effects on sample collection.

At each site, the soil was hand-augered approximately 30.5 cm deep and a fast-setting cement was poured in. A pole to mount the BSNE samplers was driven into the hole and allowed to set over a period of 24 hours. This prevents introduced error from human activity as dust is kicked up from installation. After the 24 hours, two BSNE samplers were installed on each pole. One sampler was placed

Figure 3.1: BSNE sampler setup at the unremediated section site

20 centimeters above the soil and another at one meter. These height ranges represent a value slightly above the lowest height a BSNE sampler is effective (15 cm) [12] and the maximum height generally reached by saltating particles in areas of high wind speeds [39]. The two heights allow for vertical integration of horizontal dust flux to account for differences in particle saltation heights.

Sampling occurred on a bi-weekly basis with the first sample collection occurring on August 2nd, 2021 and collection ending on September 27th, 2021. The first collection was stalled by three days past the two-week mark due to severe flooding making the site inaccessible but continued regularly from then on. During collection on September 13th, the one-meter sampler at the background site was found to be damaged from desert heat and had to be removed from site. If there was no visible sediment in a sampler during collection, the sampler was returned to the mounted pole without disturbance. To collect samples, the BSNE samplers were approached from behind their opening to minimize interference from soil suspended from walking. The samplers were removed from the pole and rinsed out into sample bottles with distilled deionized water. The bottle was then labelled with the time and date of collection. Sample bottles were also labelled with the sampling site (UR or B) and sampler height (e.g. B20 represents a background sample site collection from the 20 cm height sampler).

3.2 Sample Processing

Collected sample bottles were rinsed out into a clean preweighted 100 milliliter beaker with distilled deionized water. Each beaker was labelled for a respective sampler site and height in centimeters (B20, B100, UR20, UR100). The beakers were then placed into an oven set at 100 degrees Celsius until the water was fully evaporated and the remaining soil was dried to mass-stability. The beakers containing the samplers were then weighed and the pre-tared mass of the empty beaker subtracted. Using the collected mass, horizontal mass flux was calculated for each sampler. Vertical mass flux was then estimated using an emissions factor of 5%, based conservatively on the framework of Whicker et al (2021).

3.3 Interpretation of Historic Soil and Climate Samples

Historic soil sample data was provided from areas proximal to each sampling site (See Figure 2.3). The data are presented as reported by the analytic lab. These samples were collected in the window between March 21st, 2018 to April 6th, 2018. Soil samples reported concentrations of Ra-226 and Th-230 in pCi/g alongside total propagated uncertainty (TPU). These concentrations and total propagated uncertainties were averaged to represent a site.

Soil samples were attributed to either the B or UR sampling sites based on proximity. This was determined by their coordinate locations relative to the sampling sites. Soil sampling locations and reported Ra-226 concentrations are available for reference in Appendix A.

Meteorological data was sourced from an EPA and NRC approved tower that began collecting data on March 31st, 2021. The ten-meter tall tower collects data hourly. All parameters, wind speed and direction, precipitation, relative humidity, and barometric pressure, are collected at the ten meter height. Temperature is recorded at ten and two meters. Since CAP88 requires absolute humidity rather than relative humidity, the average relative humidity was converted to estimate annual absolute humidity using the following equation:

$$A = \frac{C * P_w}{T} \tag{3.1}$$

Where:

- A = Absolute Humidity (g/m^3)
- C = Constant ($2.1667 \frac{gK}{J}$)
- P_w = Vapour Pressure (Pa)
- T = Temperature (K)

All data was averaged from beginning of data collection to when data was pulled on October 6, 2021 to capture an "average" year onsite. Two sets of meteorological data was used for modelling - the total available data extrapolated to a year and the meteorological data only from the sampling period extrapolated to a year. This is due to the more intense weather that occurs during the summer (when sampling occurred) that may result in increased saltation and suspension.

Site	Precipitation ($cm/year$)	Ambient Temp (C)	Absolute Humidity (g/m^3)	Wind-speed (m/s)
Sampling	23.92	19.10	5.22	2.73
Total	15.05	16.97	4.77	3.35

Table 3.1: Ambrosia Lake West Meteorological Data

3.4 Vertical Flux Integration

Both horizontal and vertical mass fluxes determined for each sampling event for a site were height-integrated using a computer software called CurveExpert. Fryrear described a theoretical expression first authored by Stout that determines saltation flow (horizontal mass flux) [13]:

$$f = \text{fo}(1 + \frac{y}{\sigma})^{\beta} \tag{3.2}$$

where:

- f = Soil mass at height y, kg/m^2
- fo = Soil mass moving immediately above the soil surface at a height interval of 0 to 3 mm, kg/m^2
- y = Height above soil surface, m
- σ = Height below which 50% of total mass flow in which saltation occurs, m
- β = Dimensionless power term describing the slope of relationship between y and f

.

To solve 3.4 using site-specific data, a surface creep sample is needed. Without infrastructure to collect a surface creep sample, Fryrear suggests using a fitting software to determine $fo, \sigma, and \beta$. Equation 3.4 requires at minimum three degrees of freedom to fit the three variables. Given the two measurement heights (fulfilling variable f of the equation), there are not enough data points between the two heights to uniquely estimate the fit curve. An infinite number of fit variables $fo, \sigma, and \beta$ may be estimated with the data. Therefore, a linear regression was used to estimate the curve and uncertainty. All observations for each location (B and UR) were used to run the linear regression. Using the standard error reported by CurveExpert, a 95% confidence interval was created. Using +/- 2-σ in the confidence interval allowed for accountment of variability in vertical mass-flux measurements.

3.5 CAP-88 Modelling

The CAP-88 V4.1 data set was used to create deposition models. The run type was set to a population of adults with the reference city population file of the Nevada Test Site's 1980 census used to represent Ambrosia Lake's remote and sparsely populated locality. The closest populated area is the village of San Mateo, approximately 12 miles northeast of the Ambrosia Lake facility. San Mateo's population is approximately 139 people [7].

A meteorological data file for Grants, New Mexico is available to use in the model. It would be closely representative of the site conditions as Grants is 25

miles southeast of the facility. The wind file from the Grants was selected for use in the model while annual precipitation, average windspeed, ambient temperature, and absolute humidity were input from onsite measurements. Lid height was set to 1000 meters, which is the default for CAP-88. All data was modeled in CAP-88 using the total available meteorological data and then again using meteorological data only from the sampling period. This accounts for differences in weather since sampling occurred during the summer season.

The source-type was set to be an area source with a height of 0 meters and area of 26015.53 square meters. The BSNE sampler is standardized against a circular field of a 91-meter radius, so the area of this field serves as the source radius [37]. CAP-88 automatically rounded the area to 26020 square meters.

The plume type was set to a momentum plume to represent wind gusts of a certain exit velocity suspending sediment. The exit velocity was set to 1 cm/sec representative of a dynamic shear stress threshold velocity in which saltation is maintained.

Agricultural settings were set to be representative of consumption rates in the state of New Mexico, but were otherwise kept to default settings provided by CAP-88. The food source was set to a "rural" setting given the remote and rural location of the Ambrosia Lake facility.

Ra-226 was input as the released nuclide in particulate form. The "type" setting, referring to the type of the nuclide's chemical form (Fast, Medium, Slow, Gas, or Vapor) and size were set to the default.

The release rate input is the product of the following equation:

$$RR = VMF * C * A \tag{3.3}$$

Where:

- RR = Release Rate ($Ci/year$)
- VMF = Vertical Mass Flux ($\frac{g}{m^2 * year}$)
- C = Mean Soil Activity Concentration (Ci/g)
- A = Area of Contamination (m^2)

These inputs allow for a report to be run which reports estimated downwind deposition representative of the site. Several different vertical mass fluxes were input to model different release rate scenarios: the height integrated mass-flux as well as flux from 20 and 100 cm.

3.6 Sources of Error and Error Propagation

Error is introduced into this experiment which is analytically-derived by nature from uncertainties in measurements and from the capacity of the modeling software. Given the non-stochastic nature of CAP-88, no error is reported by the software. That is, the same inputs in CAP-88 will always generate the same outputs. To account for uncertainty, several extra runs of CAP-88 were generated.

Soils data was collected onsite which is plugged into CAP-88 as the averaged source term. However, no direct gamma measurements were recorded at the sampler locations and may not represent their specific micro-ecosystem. Each soil sample measured Ra-226 and Th-230 concentrations in picoCuries per gram (pCi/g) and included a total propagated uncertainty (TPU) provided by the laboratory that processes the soil samples. Total propagated uncertainty is defined as the combined standard uncertainty and estimated covariance. It represents a good estimate of the "true" standard uncertainty of the soil concentration.

Measurement collection from the BSNE resulted in samples of very small mass (on the order of milligrams). While the BSNE sampler has a typical sampling efficiency of 90% in perfect wind-tunnel like settings, it may vary in reality and is difficult to measure without a wind-tunnel. Any errors from these small samples would be represented in in a larger scale in the resulting models. Furthermore, the the scale used to mass the samples had a standard error of +/- 0.002 grams.

For each CAP-88 model run (at each site: the 20 cm average flux, 100 cm height average flux, and the height-integrated flux) a "low" and "high" CAP-88 model was generated. The "low" run for the 20cm and 100cm models for each site included an averaged activity concentration that was two average TPU less than the original model and accountment for measuring uncertainty by subtracting 0.004 grams from the measured mass (which in turn affects estimated VMF). The "low" models represent conditions in which there is less soil flux and lower soil activity concentrations. For the height-integrated models, the "low" flux was determined by taking the confidence interval of the fit-equation from 0 to 100 cm and integrating

a mass-flux two standard-errors below the original fit. The process for varying the activity concentration remained the same. The "high" runs repeated this process, but with an increase of two standard errors for each concentration and flux.

While the Ambrosia Lake site is in very close proximity to Grants, site-specific data including wind speed, wind direction, relative humidity, barometric pressure, and precipitation is available to allow for more accurate model output. Even so, the present meteorological station onsite is some distance from the sampler sites and may not account for fluctuations specific to sampler site micro-climates. Severe flooding resulting from intense heavy rain at the Ambrosia Lake site occurred within the first four weeks of sampling. Precipitation affects saltation by causing splash-saltation when raindrops impact upon soil, forcing it upwards (See Figure 3.2) while trapping suspendable soil due to its high moisture content [10]. CAP-88 is limited in its abilities to account for impacts of splash-saltation. Future studies could examine the impacts of heavy desert rain alone on suspension.

Some sampling events would be skipped due to no visible dust mass collected in the sampler, causing lapses in data. One of the BSNE samplers became damaged in the arid climate and was taken out before the final sample set was collected, leaving a lapse in data. This removed potential information that could have better characterized the site. Due to time constraints, sampling was not able to occur over the span of a year to get an annual snapshot of the site. A longer sampling period, more samplers, and more sampling sites would allow for more representative data in a model.

Figure 3.2: Splash Saltation Impacts Visualized on the Underside of a BSNE Sampler

Chapter 4: Results

4.1 BSNE Sampler Data

Figure 4.1 summarizes sample data collected from the BSNE samplers, including estimation of HMF and VMF. Climactic conditions for each sampling event are also described.

Sample Set	Collection Date	Collection Time	Sample period (d)	Sample Site	Sampler Height	Sample Mass (g)	Beaker Mass	Dust Mass (g)	Sample period (s)	HMF (g/m2*s)	VMF (g/m2*s)	Weather conditions	Notes
1	8/2/2021	1:24 PM	17	Background	20 cm	117.643	117.038	0.605	1468800	0.000411901	2.0595E-05	During collection: Dry - rain the past week	Sample collected late due to flooding and storms which may affect data collected
	8/2/2021			Background	100 cm	N/A	119.077					During collection: Dry - rain the past week	Sample not collected - insufficient dust mass to measure (.1 g)
	8/2/2021	12:54 PM	17	Unremediated	20 cm	117.864	115.257	2.607	1468800	0.001774918	8.87459E-05	During collection: Dry - rain the past week	Sample collected late due to flooding and storms which may affect data collected
	8/2/2021	1:15 PM	17	Unremediated	100 cm	117.675	116.758	0.917	1468800	0.000624319	3.1216E-05	During collection: Dry - rain the past week	Sample collected late due to flooding and storms which may affect data collected
2	8/16/2021	11:42 AM	14	Background	20 cm	117.803	117.038	0.765	1209600	0.00063244	3.1622E-05	Dry, no wind	
	8/16/2021	11:45 AM	28	Background	100 cm	119.245	119.076	0.169	2419200	6.98578E-05	3.49289E-06	Dry, no wind	Collection over 4 weeks (skipped 8/2)
	8/16/2021	11:12 AM	14	Unremediated	20 cm	116.679	115.257	1.422	1209600	0.001175595	5.87798E-05	Dry, no wind	
	8/16/2021	11:18 AM	14	Unremediated	100 cm	116.939	116.758	0.181	1209600	0.000149636	7.48181E-06	Dry, no wind	
3	8/30/2021	11:10 AM	14	Background	20 cm	117.776	117.037	0.739	1209600	0.000610946	3.05473E-05	Dry, no wind	
	8/30/2021	11:12 AM	14	Background	100 cm	119.173	119.077	0.096	1209600	7.93651E-05	3.96825E-06	Dry, no wind	
	8/30/2021	10:46 AM	14	Unremediated	20 cm	116.403	115.257	1.146	1209600	0.000947421	4.7371E-05	Dry, no wind	
	8/30/2021	10:49 AM	14	Unremediated	100 cm	116.818	116.761	0.057	1209600	4.7123E-05	2.35615E-06	Dry, no wind	
4	9/13/2021	1107	14	Background	20 cm	117.123	117.038	0.085	1209600	7.02712E-05	3.51356E-06	Dry, no wind	
	9/13/2021			Background	100 cm							Dry, no wind	Sampler damaged
	9/13/2021	1045	14	Unremediated	20 cm	115.312	115.248	0.064	1209600	5.29101E-05	2.6455E-06	Dry, no wind	
	9/13/2021			Unremediated	100 cm							Dry, no wind	Not collected due to insufficient mass
5	9/27/2021	1036	14	Background	20 cm	117.144	117.035	0.109	1209600	9.01124E-05	4.50562E-06	Wet from previous rain	
	9/27/2021			Background	100 cm							Sampler damaged	
	9/27/2021	1050	14	Unremediated	20 cm	116.995	116.68	0.315	1209600	0.000260417	1.30208E-05	Wet from previous rain	Beakers swapped (UR 20 and 100)
	9/27/2021	1050	14	Unremediated	100 cm	115.304	115.248	0.056	1209600	4.62963E-05	2.31481E-06	Wet from previous rain	Beakers swapped (UR 20 and 100)

Figure 4.1: Sampling Event Data Summary

4.2 Mass Flux Measurements

The average horizontal mass fluxes ("low" and "high" runs to account for variability included) measured by the BSNE samplers and their estimated vertical mass fluxes are included in the Tables 4.1 through 4.4 below. The weighed masses used to calculate mass flux are represented in Figure 4.1.

Sampler	"Low" Average HMF (g / m^2 s)	Average HMF (g / m^2 s)	"High" Average HMF (g / m^2 s)
20 cm	3.59E-04	3.63E-04	3.66E-04
100 cm	7.21E-05	7.46E-05	7.71E-05

Table 4.1: Average Horizontal Mass Fluxes for the Background Sampling Site

Sampler	"Low" Average VMF (g / m^2 s)	Average VMF (g / m^2 s)	"High" Average VMF (g / m^2 s)
20 cm	1.801E-05	1.82E-05	1.83E-05
100 cm	3.616E-06	3.73E-06	3.85E-06

Table 4.2: Estimated Average Vertical Mass Fluxes for the Background Sampling Site

Sampler	"Low" Average HMF (g / m^2 s)	Average HMF (g / m^2 s)	"High" Average HMF (g / m^2 s)
20 cm	8.39E-04	8.42E-04	8.45E-04
100 cm	2.13E-04	2.17E-04	2.20E-04

Table 4.3: Average Horizontal Mass Fluxes for the Unremediated Sampling Site

Sampler	"Low" Average VMF (g / m^2 s)	Average VMF (g / m^2 s)	"High" Average VMF (g / m^2 s)
20 cm	4.20E-05	4.21E-05	4.23E-05
100 cm	1.07E-05	1.08E-05	1.10E-05

Table 4.4: Estimated Average Vertical Mass Fluxes for the Unremediated Sampling Site

To height-integrate the two samplers at a site, a linear regression of the BSNE data was created using CurveExpert. The equation fit to the two variables (a and b) of the linear regression as follows:

$$y = bx + a \tag{4.1}$$

where:

- y = Soil Mass, (kg/m^2)
- b = Fit Slope of Regression
- x = Sampler Height, (m)
- a = Fit Y-Intercept of Regression

The fit-coefficients were then plugged into the equation and integrated from 0 to 100 cm. Results from the CurveExpert fitting and related calculus are recorded in Tables 4.5, 4.6, and 4.7 below:

Standard error and correlation coefficient (R^2) are only reported for the average background and unremediated fits, as these parameters were used to then determine fit-coefficients for the "low" and "high" calculations by construction of

Sample Site	a	b	Standard Error	R^2
"Low" Background	8.63E-02	-1.22E+00	n/a	n/a
Background	5.43E-01	-4.10E-01	3.03E-01	5.01E-01
"High" Background	9.99E-01	4.04E-01	n/a	n/a
"Low" Unremediated	2.17E-01	-2.61E+00	n/a	n/a
Unremediated	1.31E+00	-1.01E+00	8.09E-01	4.91E-01
"High" Unremediated	2.41E+00	5.94E-01	n/a	n/a

Table 4.5: Fit Coefficients For BSNE Mass Flux Height-Integration

a $2-\sigma$ confidence interval. The negative mass fluxes calculated in the Tables 4.6 and 4.7 result in an impossible negative release rate. Rather than omitting or assuming a release rate of zero, the minimum value for release rates (1E-25 Ci/year) in CAP-88 was used. Tabulated release rates for all model runs are found in Figure 4.4.

Figures 4.2 and 4.3 show the outputs of CurveExpert for the Background and Unremediated data sets, respectively.

Sample Site	"Low" HMF	Horizontal Mass Flux	"High" HMF
Background	-4.35E-04	2.79E-04	9.93E-04
Unremediated	-9.00E-04	6.68E-04	2.24E-03

Table 4.6: Average Height-Integrated Horizontal Mass Fluxes for Each Site

Sample Site	"Low" VMF	Vertical Mass Flux	"High" VMF
Background	-2.17E-05	1.40E-05	4.96E-05
Unremediated	-4.50E-05	3.34E-05	1.12E-04

Table 4.7: Average Height-Integrated Vertical Mass Fluxes for Each Site

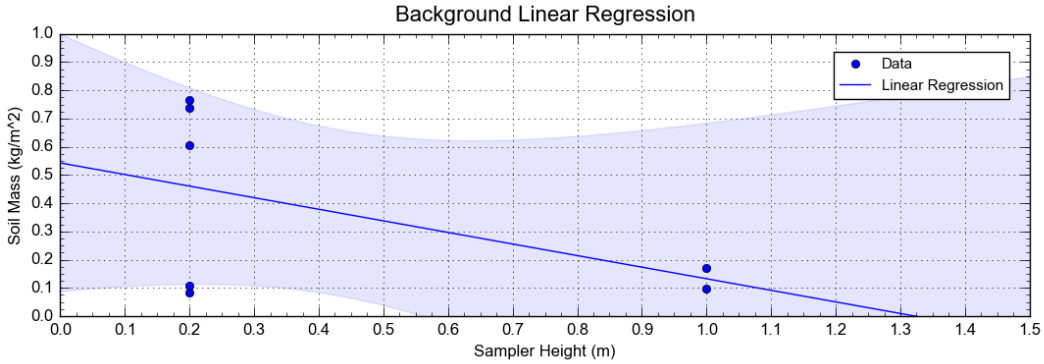

Figure 4.2: CurveExpert Output for Background Data

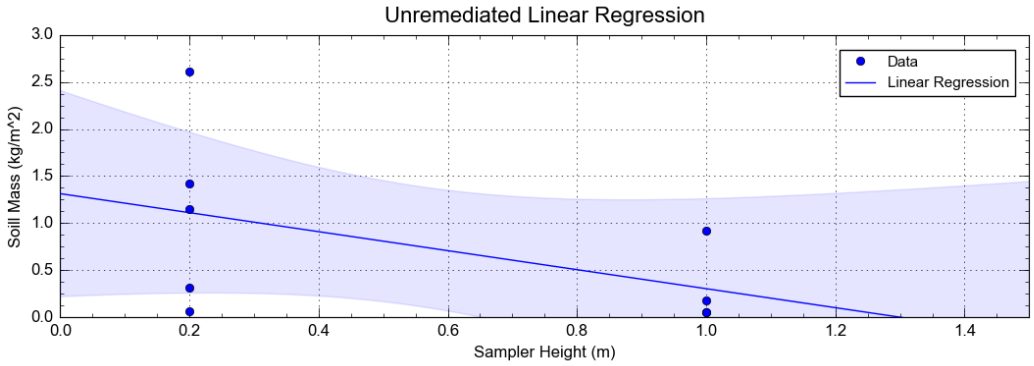

Figure 4.3: CurveExpert Output for Unremediated Data

4.3 CAP-88 Inputs

This chapter contains a summary of the inputs used for to create each CAP-88 model run for this study.

Background	Annual precip (cm/year)	Annual ambient temp (Celsius)	Absolute Humidity (g/cu meter)	Low Ra-226 RR (Ci/y)	Ra-226 RR (Ci/y)	High Ra-226 RR (Ci/y)
20 cm total met	15.05593341	16.97228693	4.77296015	1.00741E-05	1.26577E-05	1.78655E-05
100 cm total met	15.05593341	16.97228693	4.77296015	1.50727E-06	2.60072E-06	3.75973E-06
20 cm sampling met	23.91918	19.101775	5.218201551	1.00741E-05	1.26577E-05	1.78655E-05
100 cm sampling met	23.91918	19.101775	5.218201551	1.50727E-06	2.60072E-06	3.75973E-06
integrated mass flux total met	15.05593341	16.97228693	4.77296015	-3.02887E-06	1.94467E-06	4.07259E-05
integrated mass flux sampling met	23.91918	19.101775	5.218201551	-3.03E-06	1.94467E-06	4.07259E-05
Unremediated	Annual precip (cm/year)	Annual ambient temp (Celsius)	Absolute Humidity (g/cu meter)	Low Ra-226 RR (Ci/y)	Ra-226 RR (Ci/y)	High Ra-226 RR (Ci/y)
20 cm total met	15.05593341	16.97228693	4.77296015	8.59481E-05	0.000108282	0.000130782
100 cm total met	15.05593341	16.97228693	4.77296015	2.18883E-05	2.7897E-05	3.40326E-05
20 cm sampling met	23.91918	19.101775	5.218201551	8.59481E-05	0.000108282	0.000130782
100 cm sampling met	23.91918	19.101775	5.218201551	2.18883E-05	2.7897E-05	3.40326E-05
integrated mass flux total met	15.05593341	16.97228693	4.77296015	-1.17683E-05	8.72441E-06	2.92171E-05
integrated mass flux sampling met	23.91918	19.101775	5.218201551	-1.17683E-05	8.72441E-06	2.92171E-05

Figure 4.4: CAP-88 Inputs for All Model Runs

4.4 Deposition Rates

CAP-88's environmental fate and transport simulation reports result in information on dose and risk to individuals nearby from low-level chronic exposure, agricultural uptake and concentrations in food, and concentrations deposited in both soil and air. The most useful data reported by CAP-88 are ground deposition rates (combined wet and dry deposition rates) in 16 directions from 250 to 70,000 meters. These deposition rates were averaged by direction to account for instantaneous changes that would occur in reality. Average ground deposition rates of Ra-226 for each CAP-88 run ("low" and "high" variability runs included) are listed in Appendix B, Tables B.1 through B.12.

Chapter 5: Discussion

5.1 Analysis and Comparison of Deposition Rates

Higher deposition rates are expected for models representative of conditions most conducive to saltative (and therefore resuspensive) action. This was confirmed by higher deposition rates reported for the 20 cm samplers at both sites, higher deposition rates reported for the unremediated sampling site, and higher deposition rates for all +2 σ model runs. This is true for all averaged deposition rates in all directions and corresponds to lower deposition rates comparatively for the 100 cm samplers, the background sampling site, and the average and -2σ model runs. Given the more intense summertime weather during the sampling period, higher deposition rates were observed for the runs using the sampling meteorological data compared to the total available meteorological data. This is true for all model runs, despite the higher average wind-speed for the total available meteorological data. This is likely due to the differences in precipitation, absolute humidity, and ambient temperature influencing saltative wind-patterns.

Higher average ground deposition rates prevail in the SE wind direction for all model runs, though SSW is shown to prevail onsite from available meteorological data. This is likely due to the wind file for Grants, New Mexico used in CAP88 which disallows a prevailing wind direction to be set. The highest average depo-

sition rates reported out of all runs ("Low", Average, and "High") were all in the SE direction. For the all "Low", Average, and "High" runs, the UR20 runs with sampling met data have the highest deposition rates (See Table B.7).

All deposition rates reported were generally very small for both sites regardless of meteorological data or sampler height (on the order of E-36 up to E-13). At the surface, these deposition rates suggest a very long time-span of ambient deposition must occur before any impacts are visible onsite.

5.2 Potential for Impact on Site Remediation Efforts

Returning to the criterion of concern, 10 CFR 40, Appendix A, Criterion 6(6), in which average soil concentrations in the first 15 centimeters of soil in 100 square meters can not be in excess of 5 pCi/g above background, a dimensional analysis was applied using the reported CAP-88 deposition rates.

Assuming a soil density of 1.6 $\frac{g}{cm^2}$, the amount of radiation deposited in "grid" (first 15 cm of 100 square meters) can be calculated to determine Ra-226 average soil concentrations. Given the very small average deposition rates reported, it's appropriate to determine the amount of Ra-226 deposited onto the ground that results in a 1 pCi/g concentration change to the grid. To calculate the time it would take for 1 pCi/g change in the area of interest, the following equations are used:

$$1\frac{pCi}{g} \text{ change} = 15 * 10^6 cm^3 * 1.6\frac{g}{cm^3} = 24 * 10^6 \, pCi \tag{5.1}$$

Equation 5.1 explains the activity of Ra-226 that can be deposited into a grid to result in 1 pCi/g change in soil concentrations. Knowing this amount, it is possible to determine the time to deposit enough activity to cause that change with the following equation:

$$T = \frac{24 * 10^6 \ pCi}{D * A} \tag{5.2}$$

Where:

- T = Time to Deposit 1 pCi/g change (seconds)
- D = Average Deposition Rate ($\frac{pCi*cm^2}{s}$)
- A = Grid Area (1,000,000 cm^2)

Taking the highest deposition rate reported, 1.84E-13 pCi/cm^2 * s, and plugging it into Equation 5.2 and converting to years results in an approximate 4.13 million years to result in a 1 pCi/g change in the grid. This is under the assumption that there will be constant deposition under the conditions of the deposition rate, which is a +2 σ "high" UR20 run under more intense ("sampling") weather parameters. The estimated date for site closure is the year 2030, a goal that is very short relative to the time it would take for a change in soil radium concentrations from deposited resuspension [8]. Therefore, under ambient conditions, the data suggests impacts from wind-blown soil to be negligible from unremediated parcels of land during periods of non-remediation.

5.3 Future Areas of Study

5.3.1 Other Applications

This study establishes a methodology for determining impacts of wind-blown soil on remediation efforts at the Ambrosia Lake West Mill facility. It can be applied to a variety of other scenarios onsite in which soil transport is of interest. On unremediated parcels of land undergoing active remediation, interference from human activity will cause an increase in suspension and consequently deposition downwind. Setting up samplers at sites during active remediation would allow for a characterization of remedial efforts' impacts on resuspension onsite.

This study could also be reapplied to determine the impact from windblown tailings, which may be several orders of magnitude higher in radium soil concentrations than those used in this study. By simply changing the average Ra-226 concentration in the CAP-88 model most conducive to resuspension (UR20 "High") from 3.13 pCi/g to a very high concentration that may be observed at the tailings pile (say an arbitrary number like 1000 pCi/g) changes the highest deposition rate from 1.84E-13 pCi/cm^2 * s to 1.65E-11 pCi/cm^2 * s. Using Equation 5.2, the time to deposit 1 pCi/g change is approximately 46,092 years.This time-span is still much longer than the expected site closure date.

Following site closure, the Department of Energy (DOE) is responsible for the Ambrosia Lake disposal site in which tailings are impounded. The Long-Term Surveillance and Maintenance (LTSM) plan will monitor the tailings pile for a minimum of 1,000 years in event of release of radioactive tailings [15]. With an

estimated deposition time of approximately 36,000 years, which is much longer than the expected LTSM period, downwind deposition of tailings is potentially negligible as well. Employing BSNE samplers atop the tailings pile and several locations downwind would allow for a more comprehensive study on impacts from wind-blown tailings onsite.

5.3.2 Other Modelling Software

Future studies may include comparing outputs from CAP-88 to similar modeling programs. Argonne National Lab's MILDOS software is a code used to estimate the impacts of airborne emissions from uranium mill operations and functions. It uses a modified Gaussian plume and input meteorological data to determine similarly to CAP-88. Wind-files are editable in MILDOS to allow for a prevailing wind-direction to be used based on meteorological data, allowing for a more accurate climate profile of the site used in modeling. Ground deposition rates are reported in Ci/m^2 or Ci/m^3 with a smaller time-step, making its ease of access for determining impacts more complicated to determine the amount of time it would take for impacts related to 10 CFR 40, Appendix A, Criterion 6(6) if deposition rates are relatively low. MILDOS additionally allows for integration with geographic information system (GIS) technology which is already employed onsite. This would assist in visualization of downwind impacts from wind-blown sediment [5].

GENII is a set of programs developed by Pacific Northwest National Lab that also estimates radionuclide concentrations in the environment from releases, in-

cluding via wind transport. A plume or puff model is used by GENII and. This would allow modeling for a scenario in which wind-blown sediment deposits onto an already contaminated parcel of land. GENII also allows for prevailing wind direction inputs that influence the results of the environmental accumulation model output. The key feature of GENII is its attentiveness to resuspension, allowing resuspension factors to be directly input into the program. Influences of vegetation and on resuspension are also considered. Ultimately, GENII is more comprehensive and has the potential to provide a better characterization of soil transport onsite. However, GENII requires additional inputs regarding soil thickness, erodibility, and air concentrations that would need additional infrastructure to be measured before a site-characteristic model could be created [29].

Comparison of CAP-88 outputs to MILDOS and GENII outputs would allow for an examination on replicability and determine if CAP-88 outputs were good measures of site characterization. Should similar results be produced, all three programs used together would provide a more comprehensive estimation of deposition rates onsite. Different results may arise from the differences in the program, methods of measurement, or randomness in weather onsite. However, these differences may also provide another reasonable estimate of resuspension onsite.

Chapter 6: Conclusion

This study utilized both radioecologic and Aeolian studies to fulfill its research objective. Wind-blown soil transport under ambient conditions at the Ambrosia Lake West Mill facility was measured using BSNE samplers, which characterized onsite resuspension. CAP-88 was used to model downwind deposition in 16 directions utilizing historic soil activity concentration data and available meteorological data collected at the facility. Ground deposition rates were then averaged and determined to have no impact on remediation efforts onsite per the criterion of concern. The results suggest wind-blown soil onsite under the most consistent and conservative conditions deposits Ra-226 in such little amounts that it is considerably negligible. The averaged ground deposition rates generated by CAP-88 suggest that the site closure goal of 2030 would be surpassed by over four million years before any measurable change in soil activity concentrations occurs. Simulating deposition by high activity wind-blown tailings and increasing soil activity concentrations from approximately 3 pCi/g to 1000 pCi/g suggests an approximate 36,000 years to deposit a 1 pCi/g change in soil. With the Department of Energy's Long-Term Surveillance and Maintenance spanning 1,000 years, it is suggested resuspended tailings would far exceed the LTSM plan before impacts occur that would exceed the criterion of concern. Further study of wind-blown tailings, including setting up BSNE samplers atop the pile and re-using this study's methodology, would allow

for more evidence to strengthen this conclusion.

Other applications for the study's methodology would allow for several different scenarios involving resuspension to be examined onsite, such as how resupension is affected by active remediation efforts or how splash-saltation may impact estimated soil suspension onsite. There is also the opportunity to compare CAP-88 ground deposition rate results with similar programs such as MILDOS and GENII, though further onsite measurements would be required to fulfill the input needs of the software to accurately characterize the site. Utilizing high-volume air concentration samplers to measure mass loading and determining depth of topsoil would provide information required to use the software appropriately.

Bibliography

[1] Environmental Protection Agency. The legacy of abandoned uranium mines in the grants mineral belt, new mexico. https://www.epa.gov/sites/default/files/2015-08/documents/uranium-mine-brochure.pdf, November 2011. (Accessed on 08/24/2021).

[2] L. R Anspaugh, J. H. Shinn, P. L. Phelps, and N. C. Kennedy. In *Resuspension and Redistribution of Plutonium in Soils*, volume 29, pages 571 – 582, February 10 1975. (Accessed on 08/18/2021).

[3] R. A. Bagnold. *The Physics of Blown Sand and Desert Dunes*. June 1941. (Accessed on 09/10/2021).

[4] Thomas E. Barchyn and Chris H. Hugenholtz. Comparison of four methods to calculate aeolian sediment transport threshold from field data: Implications for transport prediction and discussion of method evolution. *Geomorphology*, 129(3):190–203, 2011.

[5] B.M. Biwer, D.J. LePoire, S. Kamboj, and Y.-S. Chang. *Technical Manual and User's Guide for MILDOS, Version 4.1*, 11 2019.

[6] David D. Breshears, Jeffrey J. Whicker, Chris B. Zou, Jason P. Field, and Craig D. Allen. A conceptual framework for dryland aeolian sediment transport along the grassland–forest continuum: Effects of woody plant canopy cover and disturbance. *Geomorphology*, 105(1):28–38, 2009.

[7] United States Census Bureau. San mateo cdp, new mexico. https://data.census.gov/cedsci/profile?g=1600000US3569270, 2020.

[8] United States Nuclear Regulatory Commission. Rio algom - ambrosia lake, March 24 2021.

[9] Zhibao Dong, Xiaoping Liu, Hongtao Wang, and Xunming Wang. Aeolian sand transport: a wind tunnel model. *Sedimentary Geology*, 161(1):71–83, 2003.

[10] M. Dreicer, T. E. Hakonson, G.C. White, and F.W. Whicker. Rainsplash as a mechnism for soil contamination of plant surfaces. *Health Physics*, 46(1):177–187, 1984.

[11] E. J. Farrell. *Characterizing Vertical Mass Flux Profiles in Aeolian Saltation Systems*. PhD thesis, 2012.

[12] D W Fryrear. A field dust sampler. *Journal of Soil and Water Conservation*, 41:117–120, 1986.

[13] D.W Fryrear, J.E. Stout, L. J. Hagen, and E.D. Vories. Wind erosion: Field measurement and analysis. *Transactions of the ASAE*, 34, 1991.

[14] E.K. Garger, Yu.I., S. an Kuzmenko, and J. Tschiersch Sickinger. Prediction of the cs-137 activity concentration in the atmospheric surface layer of the chernobyl exclusion zone. *Journal of Environmental Radioactivity*, 110:53–58, 2012.

[15] Jacobs Engineering Group. Long-term surveillance plan for the ambrosia lake, new mexico disposal site. 11 1995.

[16] K A Higley. Atmospheric transport lecture, 2020.

[17] Yasuhito Igarashi, Mizuo Kajino, Yuji Zaizen, K. Adachi, and Masao Mikami. Atmospheric radioactivity over tsukuba, japan: a summary of three years of observations after the fdnpp accident. *Progress in Earth and Planetary Science*, 2, 12 2015.

[18] J. D. Iversen and B.R. White. Saltation threshold on earth, mars and venus. *Sedimentology*, 29(1):111–119, 1982.

[19] M. Kajino, M. Ishizuka, Y. Igarashi, K. Kita, C. Yoshikawa, and M. Inatsu. Long-term assessment of airborne radiocesium after the fukushima nuclear accident: Re-suspension from bare soil and forest ecosystems. *Atmospheric Chemistry and Physics Discussions*, 2016.

[20] Jasper F Kok, Thomthy I Michaels Eric J R Parteli, and Diana Bou Karam. *The physics of wind-blown sand and dust*, volume 75. 2012. (Accessed on 08/25/2021).

[21] W. H. Langham. Plutonium distribution as a problem in environmental science. 1971. (Accessed on 08/18/2021).

[22] Junran Li, Gregory S. Okin, Lorelei Alvarez, and Howard Epstein. Quantitative effects of vegetation cover on wind erosion and soil nutrient loss in a desert grassland of southern new mexico, usa. *Biogeochemistry*, 85:317–332, 2007. (Accessed on 09/10/2021).

[23] GS Linsley. Resuspension of the transuranium elements-a review of existing data. 1978.

[24] Brian Littleton. *CAP88-PC VERSION 4.1 USER GUIDE*, 2019.

[25] Raleigh L. Martin and Jasper F. Kok. Distinct thresholds for the initiation and cessation of aeolian saltation from field measurements. https://agupubs.onlinelibrary.wiley.com/doi/epdf/10.1029/2017JF004416, 2018. (Accessed on 09/29/2021).

[26] Virginia T. McLemore. Uranium resources in new mexico, January 27 2020. (Accessed on 08/24/2021).

[27] Mariano J. Mendez, Roger Funk, and Daniel E. Buschiazzo. Field wind erosion measurements with big spring number eight (bsne) and modified wilson and cook (mwac) samplers. *Geomorphology*, 129(1):43–48, 2011.

[28] J. Mishima. Usaec rept. hw-83668. 1964.

[29] B.A. Napier. *GENII Version 2 Users' Guide*, 11 2012.

[30] United States Department of Agriculture. Natural Resources Conservation Service. Web soil survey. Available online at the following link: http://websoilsurvey.sc.egov.usda.gov/.

[31] K. W. Nicholson. The deposition, resuspension and weathering of Chernobyl derived material in the UK. 9(2):113–119, June 1989. Publisher: IOP Publishing.

[32] G. Rosner and R. Winkler. Long-term variation (1986-1998) of post-chernobyl sr-90, cs-137, pu-238, and 239/240-pu concentrations in air, depositions to ground, resuspension factors and resuspension rates in south germany. *The Science of the Total Environment*, 273:11–25, 2001.

[33] Yaping Shao. *Physics and Modelling of Wind Erosion*. 2008.

[34] Joseph H. Shinn, N. C. Kennedy, J. S. Koval, Bruce Clegg, and William M. Porch. Observations of dust flux in the surface boundary layer for steady and nonsteady cases. 1974.

[35] K. Stewart. *Proc. Symp. Surface Contamination*. 1964.

[36] Safety U.S. Department of Energy Office of Environment and Health. Maccs2 computer code application guidance for documented safety analysis final report, June 2004.

[37] Simon J van Donk, Xuewen Huang, Edward L Skidmore, Alan B Anderson, Dick L Gebhart, Valerie E Prehoda, and Elizabeth M Kellogg. Wind erosion from military training lands in the mojave desert, california, u.s.a. *Journal of Arid Environments*, 54(4):687–703, 2003.

[38] Jeffrey J. Whicker, David D. Breshears, and Jason P. Field. Progress on relationships between horizontal and vertical dust flux: Mathematical, empirical and risk-based perspectives - sciencedirect. *Aeolian Research*, 14:105–111, September 2014. (Accessed on 08/17/2021).

[39] Jeffrey J. Whicker, David D. Breshears, Michael McNaughton, Mary Jo Chastenet de Gery, and Christine Bullock. Radionuclide resuspension across ecosystems and environmental disturbances. *Journal of Enivronmental Radioactivity*, 233, 2021. (Accessed on 08/18/2021).

APPENDICES

Appendix A: Historic Soil Data

Figure A.2 displays soil sampling locations which determined Ra-226 activity concentrations relative to BSNE sampling locations. The data for each sample area ID and attributed BSNE sampling location is displayed in Figures A.3 and A.4. Statistical summaries of Figures A.3 and A.4 are described in Figure A.1.

Statistics	Background	Unremediated
# of samples	21	125
Average Ra-226 (pCi/g)	0.849142857	3.134032
Average Th-230 (pCi/g)	0.875190476	2.636512
Ra-226 TPU	0.169872361	0.31847469
Th-230 TPU	0	0
Average gamma	10543.57143	17447.504

Figure A.1: Soil Sample Statistics

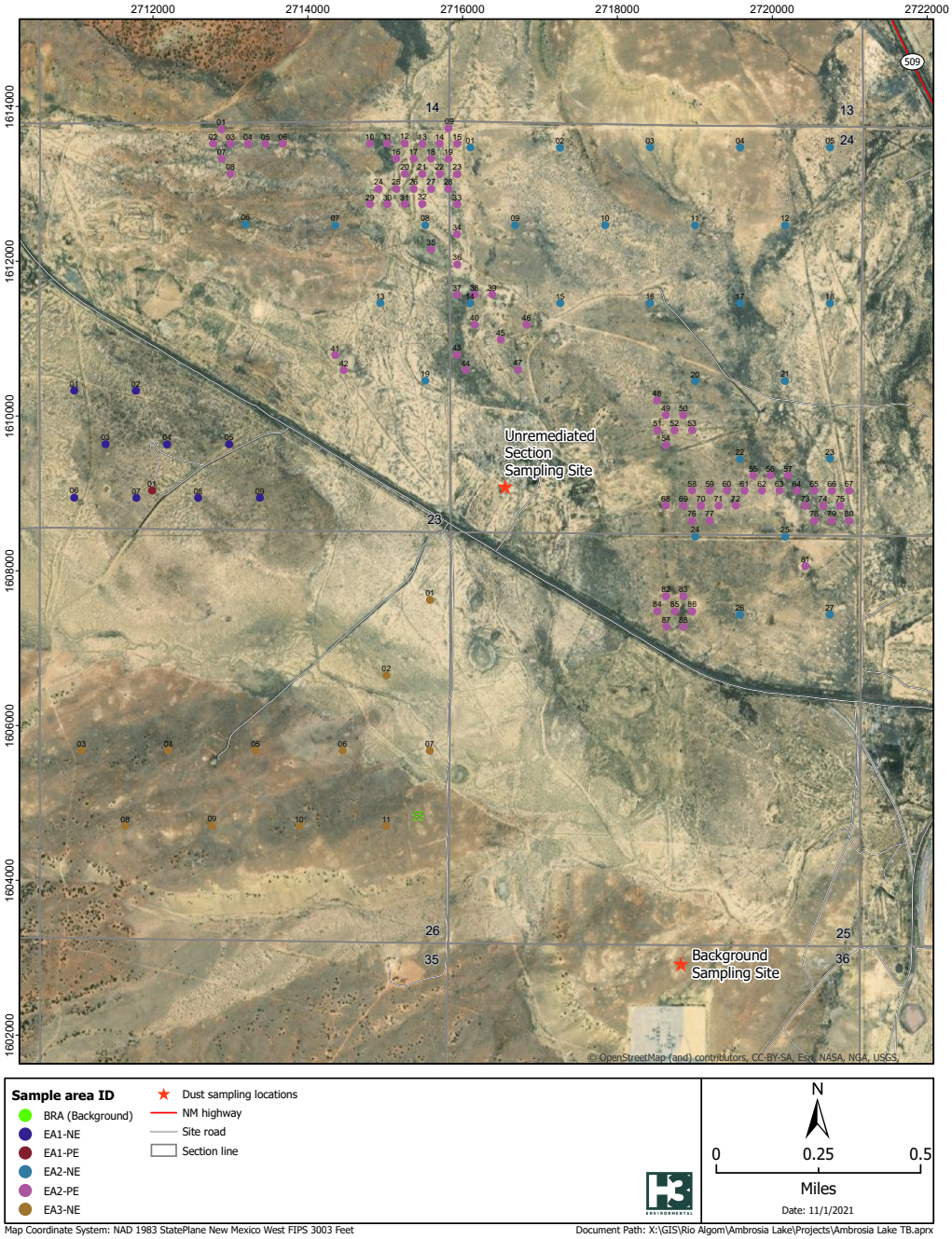

Figure A.2: Soil Activity Concentration Sampling Locations

BSNE Sampler Site	Sample ID	Ra-226 (pCi/g)	TPU (Ra-226)	Th-230 (pCi/g)	TPU (Th-230)	Measure unshielded gamma (cpm)
Background	BRA-01-0015-032118	0.961	0.171	0.978	0.542	10862
	BRA-02-0015-032118	0.731	0.121	0.641	0.361	10767
	BRA-03-0015-032118	0.912	0.124	0.873	0.388	10143
	BRA-04-0015-032118	0.722	0.119	1.03	0.452	10043
	BRA-05-0015-032118	0.83	0.12	0.708	0.425	10049
	BRA-06-0015-032118	0.934	0.139	0.761	0.392	9952
	BRA-07-0015-032118	0.731	0.117	0.494	0.329	9072
	BRA-08-0015-032118	0.746	0.109	0.551	0.299	9715
	BRA-09-0015-032118	1	0.186	0.919	0.419	10368
	BRA-10-0015-032118	0.836	0.115	0.798	0.354	9840
	EA3-NE-01-0015-032818	1.67	0.207	2.22	0.688	16979
	EA3-NE-02-0015-032818	1.49	0.332	1.33	0.632	16462
	EA3-NE-03-0015-032818	0.357	0.189	0.554	0.394	7952
	EA3-NE-04-0015-032818	0.512	0.114	0.503	0.371	7133
	EA3-NE-05-0015-032818	0.633	0.187	-0.14	0.159	9565
	EA3-NE-06-0015-032818	0.826	0.147	1.11	0.459	10497
	EA3-NE-07-0015-032818	1.61	0.208	1.83	0.668	14276
	EA3-NE-08-0015-032818	0.496	0.209	0.724	0.485	9080
	EA3-NE-09-0015-032818	0.497	0.18	0.877	0.486	9324
	EA3-NE-10-0015-032818	0.614	0.153	0.96	0.457	8847
	EA3-NE-11-0015-032818	0.724	0.156	0.658	0.468	10489

Figure A.3: Soil Sample Data Attributed to the Background Sampling Site

BSNE Sampler Site	Sample ID	Ra-226 (pCi/g)	TPU (Ra-226)	Th-230 (pCi/g)	TPU (Th-230)	Measure unshielded gamma (cpm)
Unremediated	EA2-PE-01-0015-032918	5.92	0.531	8.43	1.55	18079
	EA2-PE-02-0015-032918	3.37	0.333	3.92	1.1	17535
	EA2-PE-03-0015-032918	2.01	0.26	2.16	0.794	16486
	EA2-PE-04-0015-032918	3.14	0.324	2.71	0.695	17743
	EA2-PE-05-0015-032918	3.58	0.306	5.08	1.1	17950
	EA2-PE-06-0015-032918	2.53	0.264	2.41	0.67	13848
	EA2-PE-07-0015-032918	2.14	0.285	3.07	0.77	17475
	EA2-PE-08-0015-032918	3.45	0.295	4.59	0.946	16088
	EA2-PE-09-0015-032918	1.52	0.249	1.92	0.62	15427
	EA2-PE-10-0015-032918	2.68	0.319	2.34	0.685	15188
	EA2-PE-11-0015-032918	3.18	0.35	2.27	0.646	15938
	EA2-PE-12-0015-032918	1.59	0.27	1.82	0.599	14534
	EA1-NE-04-0015-032818	1.56	0.24	1.65	0.634	15397
	EA1-NE-05-0015-032818	1.28	0.197	1.67	0.641	14675
	EA1-NE-06-0015-032818	1.15	0.252	1.03	0.528	15599
	EA1-NE-07-0015-032818	1.1	0.202	1.56	0.593	14098
	EA1-NE-08-0015-032818	0.921	0.17	0.8	0.419	14762
	EA1-NE-09-0015-032818	0.791	0.188	1.08	0.767	12665
	EA2-NE-01-0015-032218	1.4	0.157	1.49	0.514	14052
	EA2-NE-02-0015-032218	1.09	0.177	2.05	0.657	13949
	EA2-NE-03-0015-032218	1.04	0.144	1.01	0.454	13162
	EA2-NE-04-0015-032218	1.24	0.146	1.14	0.487	12317
	EA2-NE-05-0015-032218	1.4	0.139	1.65	0.642	14917
	EA2-NE-06-0015-032218	1.29	0.133	1.22	0.479	13304
	EA2-NE-07-0015-032218	1.63	0.156	2.19	0.594	13228
	EA2-NE-08-0015-032218	1.24	0.172	1.11	0.447	15155
	EA2-NE-09-0015-032218	1.32	0.171	0.821	0.476	11960
	EA2-NE-10-0015-032218	1.54	0.202	2.07	0.664	14048
	EA2-NE-11-0015-032218	1.69	0.167	1.98	0.651	13710
	EA2-NE-12-0015-032218	1.55	0.181	1.86	0.631	12893
	EA2-NE-13-0015-032218	2.25	0.191	2.4	0.601	13943
	EA2-NE-14-0015-032218	1.13	0.167	1.49	0.499	13255
	EA2-NE-15-0015-032218	1.6	0.185	1.88	0.532	14352
	EA2-NE-16-0015-032218	1.23	0.163	2.22	0.616	14048
	EA2-NE-17-0015-032218	1.36	0.178	1.72	0.57	15036
	EA2-NE-18-0015-032218	1.55	0.174	1.93	0.608	14706
	EA2-NE-19-0015-032218	2.25	0.204	2.07	0.382	17542
	EA2-NE-20-0015-032218	1.56	0.184	1.02	0.417	14316
	EA2-NE-21-0015-032318	2.39	0.233	2.74	0.807	16250
	EA2-NE-22-0015-032318	1.11	0.165	1.36	0.535	13030
	EA2-NE-23-0015-032318	2.79	0.235	2.66	0.809	16124
	EA2-NE-24-0015-032318	1.07	0.138	1.91	0.734	12606
	EA2-NE-25-0015-032318	0.88	0.146	1.26	0.53	12654
	EA2-NE-26-0015-032318	3.08	0.253	4.44	0.992	15630
	EA2-NE-27-0015-032318	1.53	0.16	2.41	0.893	14640
	EA1-NE-01-0015-032318	1.19	0.252	1.27	0.523	15399
	EA1-NE-02-0015-032318	1.76	0.184	1.77	0.575	15976
	EA1-NE-03-0015-032318	0.953	0.128	0.486	0.339	12139
	EA2-PE-13-0015-033018	2.24	0.302	2.17	0.653	15784
	EA2-PE-14-0015-033018	2.19	0.319	2.38	0.763	17367
	EA2-PE-15-0015-033018	1.85	0.255	1.17	0.545	17624
	EA2-PE-16-0015-033018	1.94	0.257	2.26	1	17423
	EA2-PE-17-0015-033018	1.56	0.258	1.33	0.536	16056
	EA2-PE-18-0015-033018	1.32	0.28	2.5	0.739	16445
	EA2-PE-19-0015-033018	1.88	0.255	1.52	0.584	16682
	EA2-PE-20-0015-033018	2.38	0.366	2.2	0.846	16228
	EA2-PE-21-0015-033018	1.45	0.224	1.05	0.447	15850
	EA2-PE-22-0015-033018	2.36	0.273	2.59	0.742	16013
	EA2-PE-23-0015-033018	1.69	0.252	0.945	0.441	15294
	EA2-PE-24-0015-033018	2.43	0.282	1.86	0.581	16870
	EA2-PE-25-0015-033018	3.03	0.27	2.18	0.623	15809
	EA2-PE-26-0015-033018	1.41	0.243	0.815	0.417	15067

Figure A.4: Soil Sample Data Attributed to the Unremediated Sampling Site

Appendix B: CAP-88 Results

Wind Direction	"Low" Depo Rate pCi / cm^2 * s	Average Depo Rate pCi / cm^2 * s	"High" Depo Rate pCi / cm^2 * s
N	2.60E-15	3.27E-15	4.61E-15
NNW	3.99E-15	5.01E-15	7.08E-15
NW	9.35E-15	1.17E-14	1.66E-14
WNW	7.02E-15	8.82E-15	1.25E-14
W	1.58E-15	1.99E-15	2.81E-15
WSW	4.16E-16	5.23E-16	7.38E-16
SW	9.33E-16	1.17E-15	1.65E-15
SSW	1.40E-15	1.77E-15	2.49E-15
S	5.40E-15	6.78E-15	9.59E-15
SSE	1.07E-14	1.35E-14	1.90E-14
SE	1.42E-14	1.78E-14	2.51E-14
ESE	1.02E-14	1.28E-14	1.80E-14
E	5.65E-15	7.11E-15	1.00E-14
ENE	4.65E-15	5.84E-15	8.25E-15
NE	3.38E-15	4.26E-15	6.01E-15
NNE	2.43E-15	3.05E-15	4.30E-15

Table B.1: Average Ground Deposition Rates for the B20 Model Runs (Sampling Meteorological Data)

Wind Direction	"Low" Depo Rate pCi / cm^2 * s	Average Depo Rate pCi / cm^2 * s	"High" Depo Rate pCi / cm^2 * s
N	1.87E-15	2.35E-15	3.31E-15
NNW	2.88E-15	3.62E-15	5.12E-15
NW	7.17E-15	9.01E-15	1.27E-14
WNW	5.42E-15	6.80E-15	9.61E-15
W	1.13E-15	1.42E-15	2.00E-15
WSW	2.82E-16	3.54E-16	5.00E-16
SW	6.38E-16	8.02E-16	1.13E-15
SSW	9.81E-16	1.23E-15	1.74E-15
S	3.87E-15	4.86E-15	6.86E-15
SSE	7.80E-15	9.81E-15	1.39E-14
SE	1.01E-14	1.27E-14	1.79E-14
ESE	7.28E-15	9.16E-15	1.29E-14
E	4.18E-15	5.25E-15	7.41E-15
ENE	3.66E-15	4.60E-15	6.51E-15
NE	2.61E-15	3.28E-15	4.62E-15
NNE	1.85E-15	2.33E-15	3.29E-15

Table B.2: Average Ground Deposition Rates for the B20 Model Runs (Total Meteorological Data)

Wind Direction	"Low" Depo Rate pCi / cm^2 * s	Average Depo Rate pCi / cm^2 * s	"High" Depo Rate pCi / cm^2 * s
N	3.89E-16	6.71E-16	9.71E-16
NNW	5.97E-16	1.03E-15	1.49E-15
NW	1.40E-15	2.41E-15	3.49E-15
WNW	1.05E-15	1.81E-15	2.62E-15
W	2.37E-16	4.10E-16	5.93E-16
WSW	6.22E-17	1.07E-16	1.55E-16
SW	1.40E-16	2.41E-16	3.48E-16
SSW	2.10E-16	3.63E-16	5.24E-16
S	8.08E-16	1.40E-15	2.02E-15
SSE	1.60E-15	2.77E-15	4.00E-15
SE	2.12E-15	3.65E-15	5.28E-15
ESE	1.52E-15	2.62E-15	3.79E-15
E	8.47E-16	1.46E-15	2.11E-15
ENE	6.96E-16	1.20E-15	1.74E-15
NE	5.06E-16	8.75E-16	1.26E-15
NNE	3.62E-16	6.25E-16	9.05E-16

Table B.3: Average Ground Deposition Rates for the B100 Model Runs (Sampling Meteorological Data)

Wind Direction	"Low" Depo Rate pCi / cm^2 * s	Average Depo Rate pCi / cm^2 * s	"High" Depo Rate pCi / cm^2 * s
N	2.79E-16	4.82E-16	6.97E-16
NNW	4.31E-16	7.44E-16	1.08E-15
NW	1.07E-15	1.85E-15	2.68E-15
WNW	8.10E-16	1.40E-15	2.02E-15
W	1.68E-16	2.91E-16	4.21E-16
WSW	4.21E-17	7.27E-17	1.05E-16
SW	9.55E-17	1.65E-16	2.39E-16
SSW	1.47E-16	2.54E-16	3.66E-16
S	5.78E-16	9.98E-16	1.44E-15
SSE	1.17E-15	2.02E-15	2.91E-15
SE	1.51E-15	2.61E-15	3.76E-15
ESE	1.09E-15	1.88E-15	2.72E-15
E	6.25E-16	1.08E-15	1.56E-15
ENE	5.49E-16	9.47E-16	1.37E-15
NE	3.90E-16	6.73E-16	9.74E-16
NNE	2.78E-16	4.79E-16	6.92E-16

Table B.4: Average Ground Deposition Rates for the B100 Model Runs (Total Meteorological Data)

Wind Direction	"Low" Depo Rate pCi / cm^2 * s	Average Depo Rate pCi / cm^2 * s	"High" Depo Rate pCi / cm^2 * s
N	2.58E-35	5.03E-16	1.05E-14
NNW	3.96E-35	7.70E-16	1.61E-14
NW	9.28E-35	1.81E-15	3.79E-14
WNW	6.97E-35	1.36E-15	2.84E-14
W	1.58E-35	3.06E-16	6.42E-15
WSW	4.13E-36	8.03E-17	1.68E-15
SW	9.26E-36	1.80E-16	3.77E-15
SSW	1.39E-35	2.71E-16	5.67E-15
S	5.36E-35	1.04E-15	2.18E-14
SSE	1.06E-34	2.07E-15	4.33E-14
SE	1.41E-34	2.74E-15	5.72E-14
ESE	1.01E-34	1.96E-15	4.10E-14
E	5.62E-35	1.09E-15	2.29E-14
ENE	4.62E-35	8.98E-16	1.88E-14
NE	3.36E-35	6.54E-16	1.37E-14
NNE	2.41E-35	4.68E-16	9.81E-15

Table B.5: Average Ground Deposition Rates for the Integrated Background Model Runs (Sampling Meteorological Data)

Wind Direction	"Low" Depo Rate pCi / cm^2 * s	Average Depo Rate pCi / cm^2 * s	"High" Depo Rate pCi / cm^2 * s
N	1.85E-35	3.60E-16	7.54E-15
NNW	2.87E-35	5.57E-16	1.17E-14
NW	7.11E-35	1.38E-15	2.90E-14
WNW	5.37E-35	1.04E-15	2.19E-14
W	1.12E-35	2.18E-16	4.56E-15
WSW	2.79E-36	5.43E-17	1.14E-15
SW	6.33E-36	1.23E-16	2.58E-15
SSW	9.74E-36	1.90E-16	3.96E-15
S	3.84E-35	7.46E-16	1.56E-14
SSE	7.75E-35	1.51E-15	3.15E-14
SE	1.00E-34	1.95E-15	4.08E-14
ESE	7.23E-35	1.41E-15	2.95E-14
E	4.14E-35	8.07E-16	1.69E-14
ENE	3.64E-35	7.08E-16	1.48E-14
NE	2.59E-35	5.04E-16	1.05E-14
NNE	1.84E-35	3.58E-16	7.49E-15

Table B.6: Average Ground Deposition Rates for the Integrated Background Model Runs (Total Meteorological Data)

Wind Direction	"Low" Depo Rate pCi / cm^2 * s	Average Depo Rate pCi / cm^2 * s	"High" Depo Rate pCi / cm^2 * s
N	2.22E-14	2.80E-14	3.38E-14
NNW	3.41E-14	4.29E-14	5.18E-14
NW	7.99E-14	1.01E-13	1.21E-13
WNW	5.99E-14	7.55E-14	9.11E-14
W	1.35E-14	1.71E-14	2.06E-14
WSW	3.54E-15	4.48E-15	5.40E-15
SW	7.96E-15	1.00E-14	1.21E-14
SSW	1.20E-14	1.51E-14	1.82E-14
S	4.61E-14	5.81E-14	7.02E-14
SSE	9.14E-14	1.15E-13	1.39E-13
SE	1.21E-13	1.52E-13	1.84E-13
ESE	8.67E-14	1.09E-13	1.32E-13
E	4.83E-14	6.09E-14	7.36E-14
ENE	3.96E-14	5.01E-14	6.03E-14
NE	2.89E-14	3.65E-14	4.40E-14
NNE	2.07E-14	2.61E-14	3.15E-14

Table B.7: Average Ground Deposition Rates for the UR20 Model Runs (Sampling Meteorological Data)

Wind Direction	"Low" Depo Rate pCi / cm^2 * s	Average Depo Rate pCi / cm^2 * s	"High" Depo Rate pCi / cm^2 * s
N	1.59E-14	2.01E-14	2.42E-14
NNW	2.46E-14	3.10E-14	3.74E-14
NW	6.12E-14	7.72E-14	9.31E-14
WNW	4.62E-14	5.83E-14	7.03E-14
W	9.61E-15	1.21E-14	1.46E-14
WSW	2.40E-15	3.03E-15	3.65E-15
SW	5.45E-15	6.87E-15	8.28E-15
SSW	8.37E-15	1.06E-14	1.27E-14
S	3.30E-14	4.16E-14	5.02E-14
SSE	6.66E-14	8.40E-14	1.01E-13
SE	8.60E-14	1.09E-13	1.31E-13
ESE	6.22E-14	7.84E-14	9.47E-14
E	3.56E-14	4.49E-14	5.42E-14
ENE	3.13E-14	3.95E-14	4.76E-14
NE	2.23E-14	2.81E-14	3.39E-14
NNE	1.58E-14	1.99E-14	2.41E-14

Table B.8: Average Ground Deposition Rates for the UR20 Model Runs (Total Meteorological Data)

Wind Direction	"Low" Depo Rate pCi / cm^2 * s	Average Depo Rate pCi / cm^2 * s	"High" Depo Rate pCi / cm^2 * s
N	5.65E-15	7.21E-15	8.79E-15
NNW	8.68E-15	1.11E-14	1.35E-14
NW	2.03E-14	2.59E-14	3.16E-14
WNW	1.53E-14	1.95E-14	2.37E-14
W	3.45E-15	4.39E-15	5.36E-15
WSW	9.04E-16	1.15E-15	1.41E-15
SW	2.03E-15	2.59E-15	3.15E-15
SSW	3.05E-15	3.89E-15	4.74E-15
S	1.17E-14	1.50E-14	1.83E-14
SSE	2.33E-14	2.97E-14	3.62E-14
SE	3.08E-14	3.92E-14	4.78E-14
ESE	2.21E-14	2.81E-14	3.43E-14
E	1.23E-14	1.57E-14	1.91E-14
ENE	1.01E-14	1.29E-14	1.57E-14
NE	7.36E-15	9.38E-15	1.14E-14
NNE	1.36E-14	6.72E-15	7.06E-14

Table B.9: Average Ground Deposition Rates for the UR100 Model Runs (Sampling Meteorological Data)

Wind Direction	"Low" Depo Rate pCi / cm^2 * s	Average Depo Rate pCi / cm^2 * s	"High" Depo Rate pCi / cm^2 * s
N	1.59E-14	7.21E-15	8.79E-15
NNW	2.46E-14	1.11E-14	1.35E-14
NW	6.12E-14	2.59E-14	3.16E-14
WNW	4.62E-14	1.95E-14	2.37E-14
W	9.61E-15	4.39E-15	5.36E-15
WSW	2.40E-15	1.15E-15	1.41E-15
SW	5.45E-15	2.59E-15	3.15E-15
SSW	8.37E-15	3.89E-15	4.74E-15
S	3.30E-14	1.50E-14	1.83E-14
SSE	6.66E-14	2.97E-14	3.62E-14
SE	8.60E-14	3.92E-14	4.78E-14
ESE	6.22E-14	2.81E-14	3.43E-14
E	3.56E-14	1.57E-14	1.91E-14
ENE	3.13E-14	1.29E-14	1.57E-14
NE	2.23E-14	9.38E-15	1.14E-14
NNE	1.58E-14	6.72E-15	7.06E-14

Table B.10: Average Ground Deposition Rates for the UR100 Model Runs (Total Meteorological Data)

Wind Direction	"Low" Depo Rate pCi / cm^2 * s	Average Depo Rate pCi / cm^2 * s	"High" Depo Rate pCi / cm^2 * s
N	2.58E-35	2.26E-15	7.57E-15
NNW	3.96E-35	3.46E-15	1.16E-14
NW	9.28E-35	8.11E-15	2.72E-14
WNW	6.97E-35	6.08E-15	2.04E-14
W	1.58E-35	1.37E-15	4.61E-15
WSW	4.13E-36	3.60E-16	1.21E-15
SW	9.26E-36	8.08E-16	2.71E-15
SSW	1.39E-35	1.22E-15	4.07E-15
S	5.36E-35	4.69E-15	1.57E-14
SSE	1.06E-34	9.28E-15	3.11E-14
SE	1.41E-34	1.23E-14	4.11E-14
ESE	1.01E-34	8.80E-15	2.95E-14
E	5.62E-35	4.90E-15	1.64E-14
ENE	4.62E-35	4.03E-15	1.35E-14
NE	3.36E-35	2.93E-15	9.83E-15
NNE	2.41E-35	2.10E-15	7.03E-15

Table B.11: Average Ground Deposition Rates for the URIMF Model Runs (Sampling Meteorological Data)

Wind Direction	"Low" Depo Rate pCi / cm^2 * s	Average Depo Rate pCi / cm^2 * s	"High" Depo Rate pCi / cm^2 * s
N	1.85E-35	1.62E-15	7.55E-15
NNW	2.87E-35	2.50E-15	1.16E-14
NW	7.11E-35	6.21E-15	2.72E-14
WNW	5.37E-35	4.69E-15	2.04E-14
W	1.12E-35	9.76E-16	4.61E-15
WSW	2.79E-36	2.44E-16	1.21E-15
SW	6.33E-36	5.53E-16	2.71E-15
SSW	9.74E-36	8.50E-16	4.07E-15
S	3.84E-35	3.35E-15	1.57E-14
SSE	7.75E-35	6.76E-15	3.11E-14
SE	1.00E-34	8.73E-15	4.11E-14
ESE	7.23E-35	6.31E-15	2.95E-14
E	4.14E-35	3.61E-15	1.64E-14
ENE	3.64E-35	3.18E-15	1.35E-14
NE	2.59E-35	2.26E-15	9.83E-15
NNE	1.84E-35	1.60E-15	7.03E-15

Table B.12: Average Ground Deposition Rates for the URIMF Model Runs (Total Meteorological Data)